Available online at www.sciencedirect.com
SCIENCE DIRECT®
International Journal of Mass Spectrometry 227 (2003) 327–338
International Journal of Mass Spectrometry
www.elsevier.com/locate/ijms

The use of kinetic isotope effects for the determination of internal energy distributions in isolated transient species in the gas phase

František Tureček*

Department of Chemistry, Bagley Hall, Box 351700, University of Washington, Seattle, WA 98195-1700, USA

Received 7 March 2002; accepted 10 May 2002

Abstract

Isotope effects on the loss of H and D are used to estimate the internal energy distribution in transient radicals produced by collisional electron transfer in the gas phase, as studied by neutralization–reionization mass spectrometry (NRMS). Experimental intermolecular and intramolecular isotope effects are compared to those calculated by RRKM theory on ab initio potential energy surfaces and convoluted with energy distribution curves. Fitting parameters in trial energy distribution curves provides widths and maxima that are compared with the energetics of ion and neutral formation. For collisional neutralization of 2-hydroxypyridinium, 3-hydroxypyridinium, and $C(OH)_3^+$ cations by electron transfer from polarizable molecular targets, the most probable internal energy of the resulting transient radical is expressed as a simple sum of the precursor ion internal energy and the Franck–Condon energy acquired by vertical electron capture. This simple formula allows one to predict internal energies in transient neutral systems where a complete kinetic analysis of isotope effects is difficult or impractical.
© 2003 Elsevier Science B.V. All rights reserved.

Keywords: Kinetic isotope effects; RRKM calculations; Neutralization–reionization mass spectrometry; Internal energy distribution functions; Franck–Condon effects

1. Introduction

Internal energy is the major parameter that determines the rates of unimolecular dissociations of an isolated ion or neutral species in the gas phase. Unlike reactions occurring at the high pressure limit where the internal energy is governed by the Maxwell–Boltzmann distribution and characterized by temperature, the internal energy of an isolated species often cannot be related to a bulk parameter and depends on the mode of excitation. State and mode-selective excitation methods that use laser photoexcitation can deliver a known amount of energy into the isolated molecule or ion [1,2]. Likewise, long-lived ions trapped in an ion-cyclotron resonance cell can be thermalized to Boltzmann or near-Boltzmann energy distributions by radiative energy transfer with the cell walls over long trapping times [3,4]. In contrast, non-selective excitation methods, such as electron ionization, collisional activation, or collisional electron transfer, generate excited species with broad, generally non-Boltzmann, distributions of internal energy that depend on the mode of excitation and the molecular or ion system being excited. Thus, for isolated ions or neutral species that exist or dissociate on the microsecond time scale, as studied in beam experiments, the determination of

* Tel.: +1-206-685-2041; fax: +1-206-685-3478.
E-mail address: turecek@chem.washington.edu (F. Tureček).

1387-3806/03/$ – see front matter © 2003 Elsevier Science B.V. All rights reserved.
doi:10.1016/S1387-3806(03)00107-6

internal energy content and distribution is a difficult task.

Several experiments have been designed to probe internal energies of isolated species in the gas phase. Competitive dissociations are the basis of the thermometer ion method introduced by Griffiths et al. [5]. In this method, the branching ratio of two competing dissociations is monitored as a function of ion internal energy. For example, competitive loss of C_3H_7 and elimination of C_3H_6 from ionized *n*-butylbenzene has been used to probe the internal energy of the dissociating ion. The elimination, which is a rearrangement, has a lower threshold energy than the loss of C_3H_7, and so the former dissociation dominates at low ion energies. At higher internal energies, the rate constant for the loss of C_3H_7 increases more steeply than that for C_3H_6 elimination, leading to a crossing point above which the loss of C_3H_7 is faster. The branching ratio for these two dissociations thus can be used to gauge the contributions of dissociations occurring below and above the crossing point [6].

Consecutive dissociations of known thermochemistry have also been used to estimate internal energies in ions following collisional activation [7]. This method relies on step-wise dissociations of increasing endothermicity, e.g., consecutive losses of hydrogen atoms from the methane cation-radical, $CH_4^{\bullet+} \rightarrow CH_3^+ \rightarrow CH_2^{\bullet+} \rightarrow CH^+ \rightarrow C^{\bullet+}$ [7]. Because excitation initially occurs in the $CH_4^{\bullet+}$ reactant, the relative intensity of a particular fragment ion, e.g., $CH_2^{\bullet+}$, reflects the fraction of $CH_4^{\bullet+}$ that had sufficient energy to consecutively lose two hydrogen atoms, but did not have enough energy to lose the third one. The internal energy in the reactant ion is thus bracketed between the thresholds for the consecutive dissociations. $W(CO)_6^{\bullet+}$ is another thermometer ion that has been used for energy bracketing by consecutive losses of CO [8].

Collisional electron transfer to a gas-phase cation and electron detachment from an anion are used for the generation of transient neutral species by neutralization–reionization mass spectrometry (NRMS) [9–14]. It is therefore important to know the internal energies of neutral species produced by collisional neutralization. Unfortunately, the difficulties with determining internal energies in isolated ions are further exacerbated in NRMS studies. This is due to the fact that the neutral species are analyzed following collisional ionization which imparts additional energy to the ions formed and thus obscures the internal energy distribution in the neutral intermediates.

For exothermic electron transfer from an atomic donor to a cation, the energy balance can be used to determine the lower bound of the neutral excitation energy, ΔE, according to Eq. (1), where IE(N) is the ionization energy of the electron donor and RE(ion) is the recombination energy of the cation [10]. Because the collisional electron transfer at keV kinetic energies occurs in a few femtoseconds, as limited by the collision kinematics, the IE(N) and RE(ion) are best expressed as the corresponding vertical values.

$$\Delta E \geq \mathrm{RE(ion)} - \mathrm{IE(N)} \tag{1}$$

Eq. (1) rests on the assumption that the ionized target (N^+) does not receive any excitation energy, which holds reasonably well for alkali metals that have high and well known ion excitation energies, e.g., 20.24 eV for the $3p^6 \rightarrow 3p^5(^2P^\circ_{3/2})4s$ excitation in K^+, and likewise for the other alkali metal cations [15].

The situation is more complicated with near thermoneutral and endothermic electron transfer from atomic and molecular donors, where Eq. (1) does not apply. There have been a few attempts to use consecutive dissociations to estimate internal energies deposited in molecules and ions by the neutralizing and reionizing collisions. Beranova and Wesdemiotis used the $W(CO)_6^{\bullet+}$ system to investigate dissociations by consecutive losses of CO following neutralization with He, Xe, or trimethylamine and reionization with O_2 [16]. Hayakawa recently reported a similar study in which $W(CO)_{4–6}^+$ cations were converted to a mixture of $W(CO)_{0–4}^-$ anions by charge-inversion collisions with K and Cs [17]. Broad distributions of internal energies peaking at about 4 eV were found in these measurements. However, dissociations of neutral $W(CO)_{0–6}$ intermediates and ions formed therefrom were not distinguished.

A somewhat better resolution of neutral and ion dissociations has been achieved by using a system where the neutral intermediate was a very stable molecule, whereas the ion produced by collisional reionization could undergo low-energy dissociations. Methanol and methylamine cation-radicals are such systems that have been used to gauge the internal energy distributions upon NR [18]. This study, which varied the ion kinetic energy from 4000 to 8000 eV, and neutralization energetics from 2.19 eV exothermic to 0.92 eV endothermic, concluded that the energy balance according to Eq. (1) was unimportant, and most excitation upon NR originated from Franck–Condon effects on vertical electron transfer and the precursor ion internal energy. Another method that specifically targeted neutral intermediates used laser photoexcitation and photoionization to probe the population of long-lived electronic excited states in H_3 [19,20] and hypervalent ammonium radicals [21–23].

In this paper we discuss the use of competitive dissociations for estimating internal energy distributions in transient radicals produced by collisional neutralization. The experimental data, potential energy, and RRKM rate constant calculations upon which the present data analysis is based have been reported previously [24–26]. The novel feature of this approach is in that it relies on intra- and intermolecular kinetic isotope effects [27] as the probe. *Intramolecular isotope effects* are defined as being caused by different rates of competitive dissociations of an isotope-containing reactant to form chemically identical, but isotopically distinct products. *Intermolecular isotope effects* arise by different dissociation rates of distinct isotopomers of reactants having the same chemical structure. Thus, intermolecular isotope effects do not refer to competing dissociations. Both types of isotope effects are typically quantified by the relative dissociation rates, e.g., r_H/r_D ratios for dissociations involving protiated and deuterated reactants and products. The advantage of using isotope effects rests on the fact that dissociations of isotopomers have very similar transition states and hence dissociation energetics, and the reactants and/or dissociation products have very similar properties. This minimizes the effects of variations in ion structures, transition state energies, and product ionization cross-sections that caused difficulties in the previous studies. The goal of this paper is to summarize and unify data from previous experimental work and to provide a detailed analysis of internal energy deposition in three chemically different systems.

2. Results and discussion

2.1. Intermolecular isotope effects

Consider two isotopic forms of a radical, MH and MD, respectively, produced by collisional neutralization of the corresponding cations MH^+ and MD^+, respectively, that undergo unimolecular dissociation by loss of H and D, respectively. Examples of such systems are the 3-hydroxy-(1*H*,2*H*)-dihydropyrid-2-yl radical (**1H**) and its 1-D-isotopomer (**1D**) (Scheme 1a) [24], or the 2-hydroxy-(1*H*,2*H*)-dihydropyrid-2-yl radical (**2H$_2$**) and its [1-D, O-D]-isotopomer (**2D$_2$**) [25] (Scheme 1b). Following neutralization, radicals **1H** and **1D** undergo facile dissociation by loss of H-1 and D-1, respectively, to produce 3-hydroxypyridine (**1**) as a common product [24]. This experimental finding is explained by ab initio calculations of the potential energy surface (Fig. 1), that indicate that loss of H-1 (or D-1) is the lowest-energy dissociation of **1H** and **1D**, so that in the energy window between 126 and 174 kJ mol^{-1} (the hatched area in Fig. 1), loss of H-1 is the only energetically possible dissociation [24].

Because of the dissociation simplicity, the concentration of undissociated **1H**, denoted [**1H**], is given by Eq. (2), where [**1**] is the concentration of the product **1**.

$$[\mathbf{1H}] = \{[\mathbf{1H}] + [\mathbf{1}]\} \int_{E_{0,H}}^{\infty} P_H(E)\, e^{-k_{N-H}(E)\tau_H}\, dE \quad (2)$$

$P_H(E)$ is the internal energy distribution in **1H**, $k_{N-H}(E)$ is the energy-dependent unimolecular rate constant for dissociation by N–H bond cleavage, and τ_H is the time for dissociation. Likewise, the concentration of undissociated **1D**, measured separately, is given by Eq. (3), where the variables and parameters

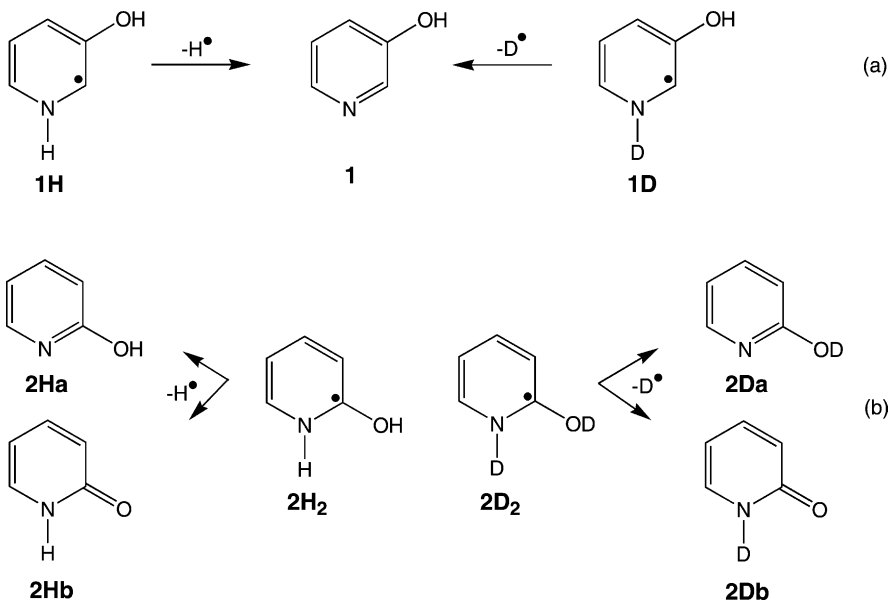

Scheme 1.

are defined as in Eq. (2).

$$[\mathbf{1D}] = \{[\mathbf{1D}] + [\mathbf{1}]\} \int_{E_{0,D}}^{\infty} P_D(E)\, e^{-k_{N-D}(E)\tau_D}\, dE \quad (3)$$

Concentrations [**1H**] and [**1**] are approximated by the relative ion intensities in the corresponding NR mass spectra, e.g., [**1H**] ∼ $I(\mathbf{1H}^+)$ and [**1**] ∼ $I(\mathbf{1}^{\bullet+})$. This rests on the assumption that **1H** and **1** have similar ionization cross-sections, so that the conversion on reionization, **1H** → $\mathbf{1H}^+$ and **1** → $\mathbf{1}^{\bullet+}$, does not introduce substantial discrimination in the ion intensities. This assumption appears to be reasonable [24], because the cross-sections for collisional ionization at keV kinetic energies follow additivity rules similar to the Fitch–Sauter rules for 70 eV electron ionization [28]. A one-hydrogen atom difference between **1H** and **1** is therefore thought to cause a negligible difference in the ionization cross-sections. Note also that one does not need to know the absolute reionization cross-sections, because Eqs. (2) and (3) use concentration ratios only. Another assumption that needs to be addressed regarding the use of ion intensities is that reionized $\mathbf{1H}^+$ and $\mathbf{1}^{\bullet+}$ dissociate to similar extent, so that the measured intensities of undissociated ions are equally proportional to the ion populations produced by reionization. This assumption is upheld by the substantial endothermicity of the $\mathbf{1H}^+$ and $\mathbf{1}^{\bullet+}$ dissociations that typically require >400 kJ mol^{-1} for pyridine, protonated pyridine, and related heterocyclic ions [24,29]. The experimental relative intensities $[\mathbf{1H}^+]/\{[\mathbf{1H}^+] + [\mathbf{1}^{\bullet+}]\}$ and $[\mathbf{1D}^+]/\{[\mathbf{1D}^+] + [\mathbf{1}^{\bullet+}]\}$ are fitted to those calculated from Eqs. (2) and (3). The calculations use the known dissociation times τ_H and τ_D and the RRKM rate constants, $k_{N-H}(E)$ and $k_{N-D}(E)$, calculated for the corresponding ab initio transition state energies, to evaluate the exponential terms in Eqs. (2) and (3). The exponentials are convoluted with trial $P(E)$ functions to provide the best fit with experiment. For simplicity, the same $P(E)$ function is considered for both **1H** and **1D**, $P(E) = P_H(E) \approx P_D(E)$. Obviously, the choice of the $P(E)$ function is important. We investigated three types of functions, i.e., a symmetrical Gaussian distribution (Eq. (4)), a truncated Boltzmann-like distribution tailing to high energies (Eq. (5)), and an inverse Boltzmann-like distribution tailing to low

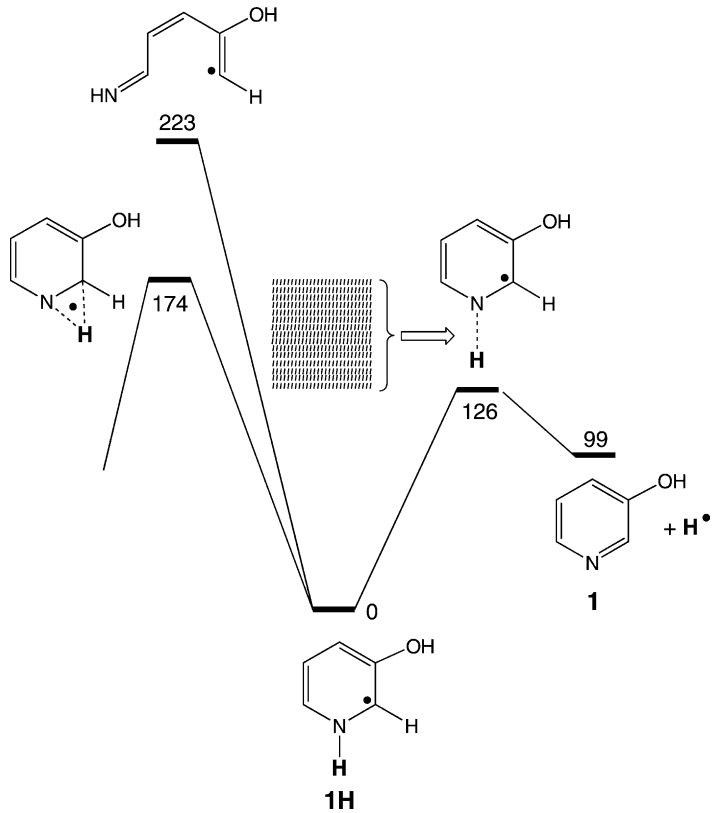

Fig. 1. Potential energy diagram (B3-PMP2/6-311G(2d,p) relative energies in kJ mol^{-1}) for hydrogen atom loss from **1H** [24].

energies (Eq. (6)).

$$P(E) = \frac{4\sqrt{\ln 2}}{W} e^{-4\sqrt{\ln 2}(E-E_0/W)^2} \quad (4)$$

$$P(E) = \frac{4(E-E_0)}{W^2} e^{-2(E-E_0/W)},$$
$$P(E \leq E_0) = 0 \quad (5)$$

$$P(E) = \frac{4(E_0-E)}{W^2} e^{-2(E_0-E/W)},$$
$$P(E \geq E_0) = 0 \quad (6)$$

All three functions are normalized such that $\int P(E)\,dE = 1$ and characterized by two parameters, one of position (E_0) and the other of width (W). In the Gaussian function (4), W is the full width at half maximum (FWHM). The Boltzmann-like function (5) has an onset at E_0, and the distribution is characterized by a maximum at $E_{max} = E_0 + W/2$, and a mean at $\langle E \rangle = E_0 + W$. The inverted Boltzmann function (6) is truncated at E_0, and is characterized by a maximum at $E_{max} = E_0 - W/2$, and a mean at $\langle E \rangle = E_0 - W$.

All three distribution functions can be fitted to reproduce the experimental isotope effects on dissociations of **1H** and **1D** within 1% relative standard deviation, which is better than the reproducibility of NRMS ion intensity measurements (5% relative). The best fit for the Gaussian function, optimized for both E_0 and W (Fig. 2), gives a broad distribution centered at $E_0 = 201$ kJ mol^{-1}. Fig. 3 shows the standard deviations for other values of E_0 that were optimized in the W coordinate only. The fit is reasonably narrow along the E_0 axis. The optimized Boltzmann-like

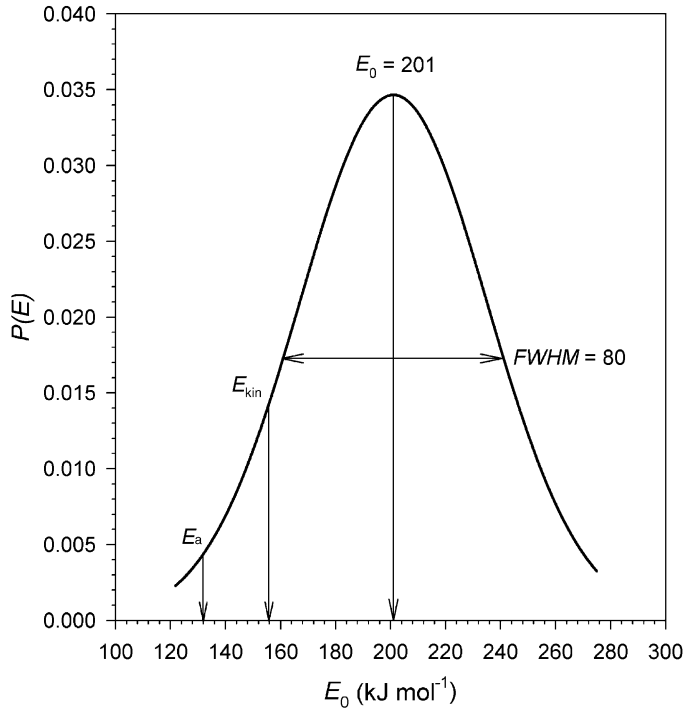

Fig. 2. Best fit Gaussian energy distribution function for dissociations of **1H** and **1D**.

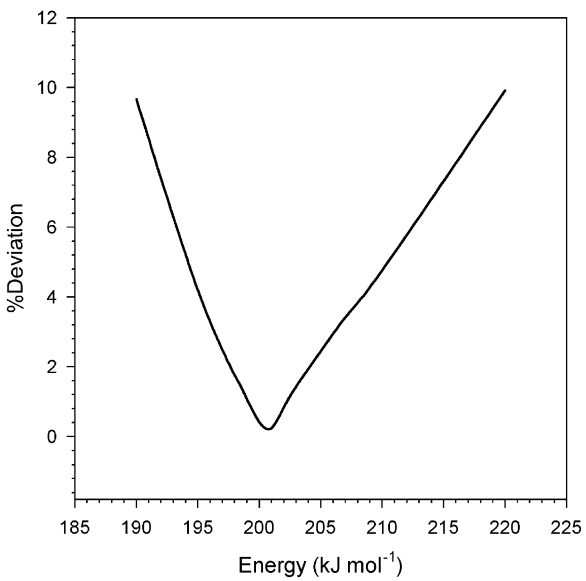

Fig. 3. Relative standard deviations for Gaussian energy distributions as a function of mean energy E_0. The width (W) has been optimized at each E_0.

(Fig. 4) and inverted Boltzmann distribution functions (Fig. 5), also gave very tight fits, as shown in Figs. 6 and 7, respectively. The Boltzmann-like distribution function ($E_0 = 145$, $W = 26\,\mathrm{kJ\,mol^{-1}}$) shows a maximum at $E_{max} = 158\,\mathrm{kJ\,mol^{-1}}$ and the mean energy at $\langle E\rangle = 171\,\mathrm{kJ\,mol^{-1}}$. The inverted Boltzmann function ($E_0 = 190$, $W = 27\,\mathrm{kJ\,mol^{-1}}$) shows a maximum at $E_{max} = 176\,\mathrm{kJ\,mol^{-1}}$, and the mean energy at $\langle E\rangle = 163\,\mathrm{kJ\,mol^{-1}}$.

Considering the dissociation kinetics, the functions offer different physical descriptions of **1H**/**1D** dissociations. The potential energy diagram in Fig. 1 shows the dissociation threshold for **1H** to be at $E_a = 126\,\mathrm{kJ\,mol^{-1}}$, so radicals with above-threshold energies are metastable and will eventually dissociate. However, because of the limited observation time scale ($\tau_H \approx \tau_D = 4.7\,\mu s$), the dissociations are subject to a kinetic shift [30]. For example, to achieve ≥50% dissociation of **1H** requires rate constants of $k_H \geq 1.5 \times 10^5\,s^{-1}$, or $\log k_H \geq 5.17$, for which the

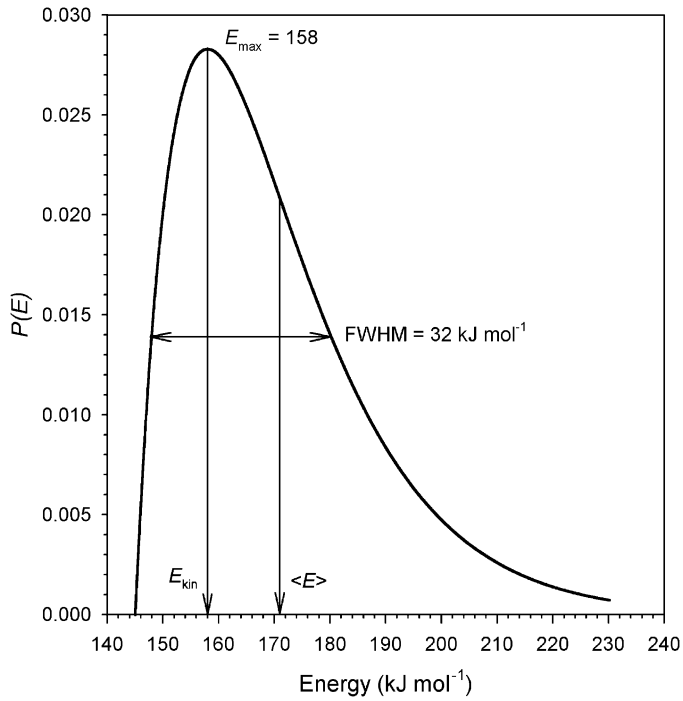

Fig. 4. Best fit Boltzmann-like energy distribution function for dissociations of **1H** and **1D**.

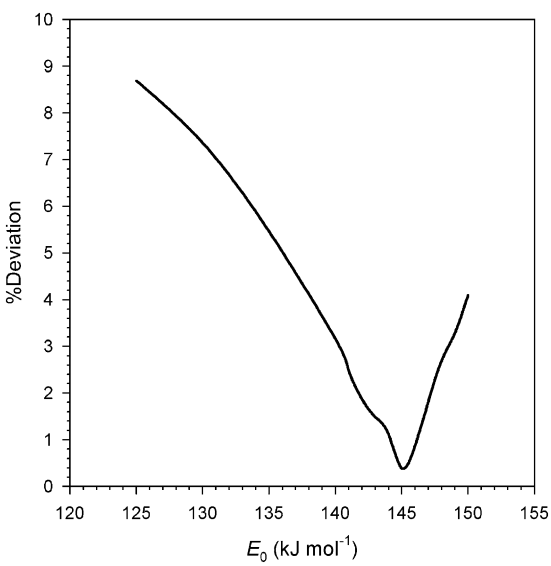

Fig. 5. Relative standard deviations for Boltzmann-like energy distributions as a function of threshold energy E_0. The width (W) has been optimized at each E_0.

RRKM calculations give an energy excess (kinetic shift) of $\Delta E = E_{kin} - E_a \geq 35\,kJ\,mol^{-1}$ [24]. These energy limits are shown as vertical arrows in Figs. 2, 4, and 5. The Gaussian and inverted Boltzmann distributions that both tail to low energies involve a small fraction of stable **1H** with internal energies of less than E_a, and also fractions of metastable **1H** with internal energies between E_a and E_{kin}. In contrast, the Boltzmann-like distribution curve starts above E_a and involves only metastable **1H**. Note that the values of E_{kin} and E_{max} coincidentally overlap in Fig. 4.

The kinetic effects on the H/D loss from **2H$_2$** and **2D$_2$** involve two competing dissociations by cleavages of the N–H, D and O–H, D bonds to give isomeric products **2Ha** and **2Hb** and/or **2Da** and **2Db** (Scheme 1b), as shown in the potential energy diagram in Fig. 8. Because the NH and OH groups in **2H$_2$** cannot be labeled separately, one can only measure intermolecular isotope effects due to combined losses of H or D, but not intramolecular isotope effects on competitive losses of N–H vs. O–D and

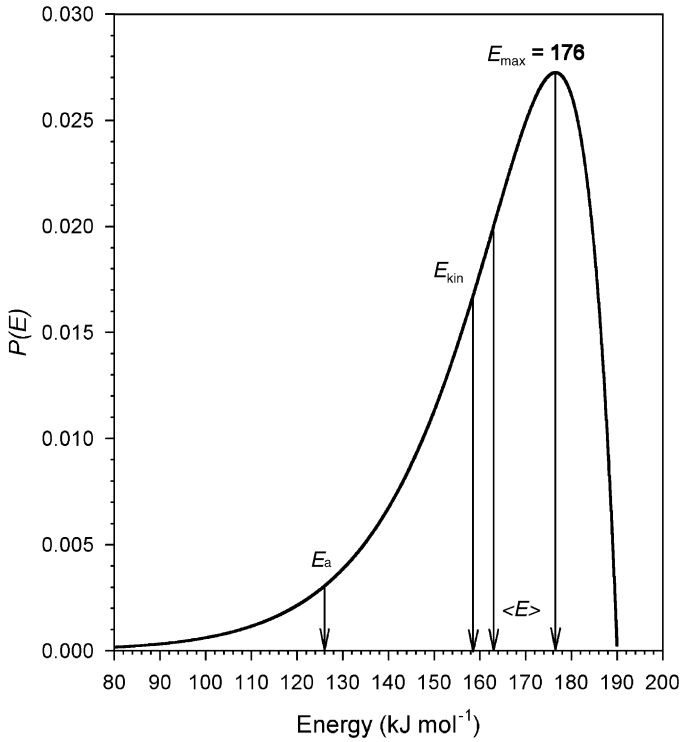

Fig. 6. Best fit inverted Boltzmann energy distribution function for dissociations of **1H** and **1D**.

vice versa. The concentrations of undissociated $\mathbf{2H_2}$ and $\mathbf{2D_2}$ are given in Eqs. (7) and (8), respectively

$$[\mathbf{2H_2}] = \{[\mathbf{2Ha}] + [\mathbf{2Hb}] + [\mathbf{2H_2}]\} \int_{E_{0,\mathrm{H}}}^{\infty} P_{\mathrm{H}}(E) \mathrm{e}^{-(k_{\mathrm{N-H}}+k_{\mathrm{O-H}})\tau_{\mathrm{H}}} \, \mathrm{d}E \qquad (7)$$

$$[\mathbf{2D_2}] = \{[\mathbf{2Da}] + [\mathbf{2Db}] + [\mathbf{2D_2}]\} \int_{E_{0,\mathrm{D}}}^{\infty} P_{\mathrm{D}}(E) \mathrm{e}^{-(k_{\mathrm{N-D}}+k_{\mathrm{O-D}})\tau_{\mathrm{D}}} \, \mathrm{d}E \qquad (8)$$

where $k_{\mathrm{N–H}}$, $k_{\mathrm{O–H}}$, $k_{\mathrm{N–D}}$, and $k_{\mathrm{O–D}}$ are the RRKM rate constants for dissociations of the respective bonds in $\mathbf{2H_2}$ and $\mathbf{2D_2}$. Note that **2Ha** and **2Hb**, and analogously **2Da** and **2Db**, are isomeric products that are not distinguished in the NR mass spectra. It is assumed that their ionization cross-sections and dissociations are similar and do not introduce serious discrimination effects in the ion intensity measurements. The very similar stabilities of **2Ha** and **2Hb** and also of the corresponding cation-radicals [25] support this assumption.Fitting Eqs. (7) and (8) with the calculated RRKM rate constants that were based on QCISD(T)/6-311+G(2d,p) transition state energies gave physically reasonable results only for the Boltzmann-like function (Eq. (5)), which showed the best fit for $E_0 = 100\,\mathrm{kJ\,mol^{-1}}$ and $W = 57\,\mathrm{kJ\,mol^{-1}}$, giving $E_{\max} = 129$ and $\langle E \rangle = 157\,\mathrm{kJ\,mol^{-1}}$ [25]. The ruggedness of the fitting is demonstrated by using RRKM rate constants that were based on B3-PMP2/6-311+G(2d,p) transition state energies [32] (Fig. 8), that gave $E_0 = 105\,\mathrm{kJ\,mol^{-1}}$ and $W = 49\,\mathrm{kJ\,mol^{-1}}$, giving $E_{\max} = 129$ and $\langle E \rangle = 154\,\mathrm{kJ\,mol^{-1}}$. Although the agreement between the experimental intensity ratios and the best fit was very good, e.g., 0.498 and 0.623 measured [25] vs. 0.496 and 0.621 calculated, and essentially insensitive to small variations in the transition state energies, similar fits could be achieved by several combinations of

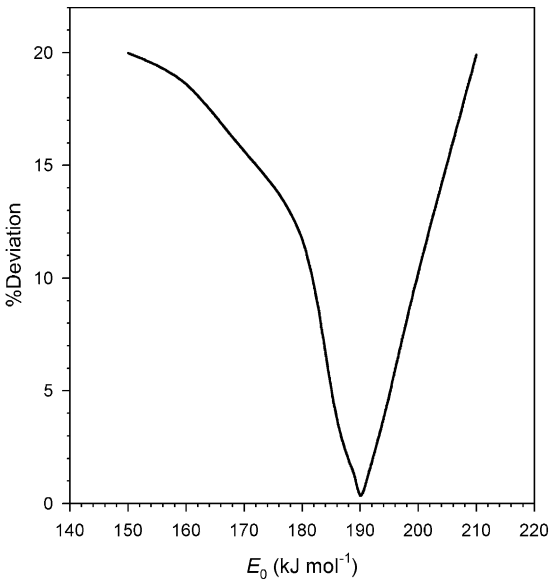

Fig. 7. Relative standard deviations for inverted Boltzmann energy distributions as a function of cut-off energy E_0. The width (W) has been optimized at each E_0.

E_0 and W, ranging from $E_0 = 95$, $W = 57\,\mathrm{kJ\,mol^{-1}}$ up to $E_0 = 115$ and $W = 40\,\mathrm{kJ\,mol^{-1}}$. These distribution curves give the E_{max} values in the range of 124–135 $\mathrm{kJ\,mol^{-1}}$ and the $\langle E \rangle$ values between 152 and 155 $\mathrm{kJ\,mol^{-1}}$. The Gaussian and inverted Boltzmann $P(E)$ functions did not give good fits for the intensity ratios within a reasonable range of internal energies, e.g., $0 \leq E \leq 250\,\mathrm{kJ\,mol^{-1}}$. Note that for **2H$_2$** the Boltzmann-like $P(E)$ function includes a fraction of stable radicals with internal energies below the lowest transition state at 125 $\mathrm{kJ\,mol^{-1}}$ (Fig. 8).

The conclusion one can make from fitting the different $P(E)$ functions is that the Boltzmann-like distribution appears to be more generally applicable, while the other functions are not. The question one has to ask is whether or not are the energy parameters obtained by fitting RRKM curves reasonable and what insight they might provide. As reported previously [24,25], the internal energy of the radicals formed by vertical electron transfer in the ground electronic state is composed of the internal energy of the precursor ion and the energy acquired as a result of Franck–Condon effects. For **1H$^+$** produced by exothermic protonation with $(CH_3)_2C{-}OH^+$ (Eq. (9)), $-\Delta H_{rxn} = \Delta PA = PA(\text{acetone}) - PA(\mathbf{1}) = 110\,\mathrm{kJ\,mol^{-1}}$ [24], the precursor

$$\mathbf{1} + (CH_3)_2C{-}OH^+ \rightarrow \mathbf{1H}^+ + (CH_3)_2C{=}O \qquad (9)$$

ion energy is limited from above by a combination of the molecule thermal internal energy ($H_T = 27\,\mathrm{kJ\,mol^{-1}}$ for **1** at the 473 K ion source temperature) and a fraction of the protonation exothermicity. The latter can be estimated from the calculated heat capacities of the conjugate base and **1H$^+$**, assuming equilibrium energy partitioning between those two products upon protonation, or by using an estimate of 80–85% partition of excess energy in the ion that was derived by Uggerud for exothermic proton transfer in a model system [31]. For **1H$^+$** and **2H$^+$**, the equilibrium-based estimates give 67–70% of ΔH_{rxn} being retained in the hydroxypyridinium ions. The Franck–Condon energy (E_{FC}) is obtained computationally as a difference between the energy of the optimized radical structure and that obtained by adding an electron to the optimized ion structure. The E_{FC} represent average values for transitions from the $v' = 0$ vibrational state of the ion, as discussed previously [18]. The estimates based on the precursor ion energy and Franck–Condon energies (Eq. (10)) thus give $E_{int} = 159$ and $129\,\mathrm{kJ\,mol^{-1}}$ for **1H** and **2H**, respectively.

$$E_{int} = E_{ion} + E_{FC} \qquad (10)$$

In the specific case of a precursor ion produced by gas-phase protonation, Eq. (10) can be formulated as Eq. (11), where H_T is enthalpy of the molecule that was protonated, and ΔPA is the protonation exothermicitiy.

$$E_{int} = H_T + 0.8\,\Delta PA + E_{FC} \qquad (11)$$

[24,25]. These estimates agree very well with the corresponding E_{max} values calculated from the isotope effects using the optimized Boltzmann-like energy distributions. Eq. (10) gives a very simple formula for the estimation of the most probable internal energy in

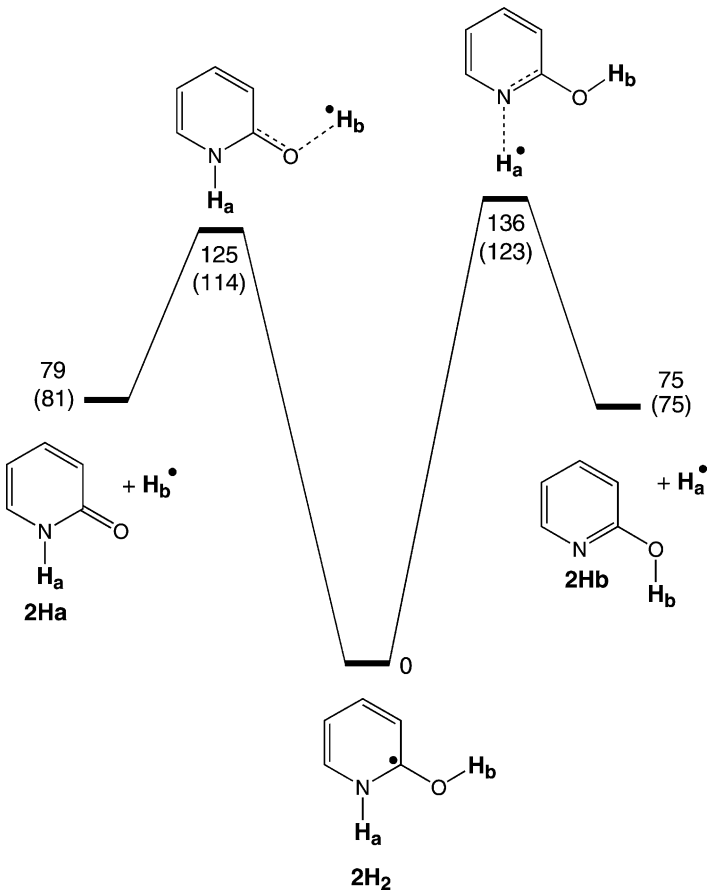

Fig. 8. Potential energy diagram (effective QCISD(T)/6-311+G(2d,p) relative energies in kJ mol^{-1}) for hydrogen atom loss from **2H** [25]. The energies in parentheses are from B3-PMP2/6-311+G(2d,p) calculations.

the neutral species produced by collisional electron transfer.

2.2. Intramolecular isotope effects

In case of competing unimolecular dissociations of an ion or neutral species involving different isotopes, the isotope effects are obtained by measuring the relative intensities of isotopomeric products in the spectrum. Because, save for the presence of different isotopes, the products are chemically identical species formed under identical experimental conditions, they can be expected to have very similar properties, so that the above-mentioned assumptions regarding the correspondence between ion intensities and concentrations are satisfied very well. An example of intramolecular isotope effects on dissociations of transient neutral species is provided by partially deuterated trihydroxymethyl radicals, **3H$_2$D** and **3HD$_2$**, that upon collisional neutralization predominantly dissociate by loss of H or D to form isotopomeric carbonic acids as shown for **3H$_2$D** (Scheme 2). [26]. The reaction scheme for **3HD$_2$** is entirely analogous to that in Scheme 2 with H replacing D in all structures and rate constant suffices. The dissociation kinetics is somewhat complicated by the fact that the radicals exist as two rapidly equilibrating conformers (syn and anti) that lose H

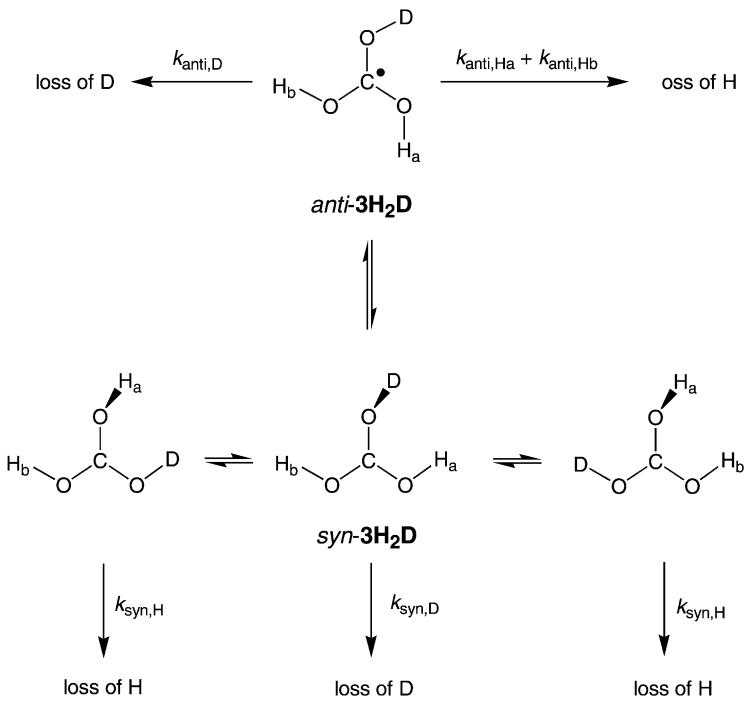

Scheme 2.

or D through distinct transition states of different symmetry [26].

Because the dissociations are competitive originating from the same reactant, the isotope effects can be expressed as ratios of the pertinent rate constants according to Eq. (12).

$$\frac{k_H}{k_D} = \frac{\int_0^{\tau_H} dt \int_{E_{a,H}}^{\infty} f_H[k_H(E), k_D(E)] \times P(E) e^{-(k_H(E)t)/\sum k(E)} dE}{\int_0^{\tau_D} dt \int_{E_{a,D}}^{\infty} f_D[k_H(E), k_D(E)] \times P(E) e^{-(k_D(E)t)/\sum k(E)} dE} \quad (12)$$

where the f_H and f_D functions are defined by Eqs. (13) and (14), respectively

$$f_H[k_H(E), k_D(E)] = \frac{x_{anti}(k_{anti,H_a} + k_{anti,H_b}) + 2x_{syn}k_{syn,H}}{x_{anti}(k_{anti,H_a} + k_{anti,H_b}) + x_{syn}(2k_{syn,H} + k_{syn,D})} \quad (13)$$

$$f_D[k_H(E), k_D(E)] = \frac{x_{anti}k_{anti,D} + x_{syn}k_{syn,D}}{x_{anti}(k_{anti,H_a} + k_{anti,H_b}) + x_{syn}(2k_{syn,H} + k_{syn,D})} \quad (14)$$

and x_{syn} and x_{anti} are the conformer molar fractions. Because the dissociations are very fast such that $k\tau \gg 1$ [26], Eq. (12) is reduced to a time-independent Eq. (15), which can be fitted with $P(E)$ functions to match the experimental isotope effects. Note that a single $P(E)$ function is used

$$\frac{k_H}{k_D} = \frac{\int_{E_{a,H}}^{\infty} f_H[k_H(E), k_D(E)]P(E)\,dE}{\int_{E_{a,D}}^{\infty} f_D[k_H(E), k_D(E)]P(E)\,dE} \quad (15)$$

for both k_D and k_H in describing intramolecular isotope effects. The best fit was obtained for a broad Boltzmann-like function with $E_0 = 110\,kJ\,mol^{-1}$ and $W = 138\,kJ\,mol^{-1}$, e.g., $k_H/k_D = 3.48$ and 0.89 for **3H$_2$D** and **3HD$_2$**, respectively, to be compared with the corresponding experimental values of 3.47 and

0.91, respectively. Hence the most probable internal energy in **3H** is $E_{max} = 110 + 138/2 = 179\,kJ\,mol^{-1}$ and $\langle E \rangle = 248\,kJ\,mol^{-1}$. The onset energy E_0 substantially exceeds the transition state energies for loss of H, which were $93\,kJ\,mol^{-1}$ from *anti*-3H and $89\,kJ\,mol^{-1}$ from *syn*-3H, in line with the complete dissociation of the radicals [26].

The E_{max} value includes the substantial Franck–Condon energy in vertical neutralization ($E_{FC} = 162\,kJ\,mol^{-1}$ [26]), leaving $17\,kJ\,mol^{-1}$ for the internal energy of the precursor trihydroxymethyl cation $\mathbf{3H}^+$, which is close to the calculated thermal energy of the ion ($H_T = 20\,kJ\,mol^{-1}$). Hence, a simple sum of E_{FC} and H_T(ion) again provides a reasonable estimate for the internal energy of the transient radicals formed by collisional electron transfer.

3. Conclusions

Analysis of kinetic isotope effects on dissociations in the NR spectra provides reasonably good estimates of internal energy distributions in transient radicals formed by vertical electron transfer in their ground electronic states. The most probable internal energy, E_{max}, can be expressed as a simple sum of the precursor ion internal energy (thermal or hyperthermal) and the Franck–Condon excitation energy acquired upon neutralization. This simple scheme was applied to and shown to hold for three different chemical systems using intermolecular and intramolecular isotope effects. The energy distributions resulting from endothermic collisional electron transfer from molecular donors differ from those estimated previously for exothermic electron transfer from alkali metal atoms.

Acknowledgements

Support for this work was provided by the National Science Foundation, Grants CHE-0090930 for experimental work and CHE-9808182 for computations.

References

[1] K. Tanaka, T. Kato, P.M. Guyon, I. Koyano, J. Chem. Phys. 77 (1982) 4441.
[2] R.J. Green, S.L. Anderson, Int. Rev. Phys. Chem. 20 (2001) 165.
[3] R.C. Dunbar, T.B. McMahon, Science (Washington, DC) 279 (1998) 194.
[4] V. Ryzhov, Y.-C. Yang, S.J. Klippenstein, R.C. Dunbar, J. Phys. Chem. A 102 (1998) 8865.
[5] I.W. Griffiths, E.S. Mukhtar, R.E. March, F.M. Harris, J.H. Beynon, Int. J. Mass Spectrom. Ion Phys. 39 (1981) 125.
[6] R.K. Boyd, F.M. Harris, J.H. Beynon, Int. J. Mass Spectrom. Ion Process. 66 (1985) 185.
[7] M.S. Kim, F.W. McLafferty, J. Am. Chem. Soc. 100 (1978) 3279.
[8] V.H. Wysocki, H.I. Kenttamaa, R.G. Cooks, Int. J. Mass Spectrom. Ion Process. 75 (1987) 181.
[9] C. Wesdemiotis, F.W. McLafferty, Chem. Rev. 87 (1987) 485.
[10] J.L. Holmes, Mass Spectrom. Rev. 18 (1989) 513.
[11] F. Tureček, Org. Mass Spectrom. 27 (1992) 1087.
[12] C.A. Schalley, G. Hornung, D. Schroder, H. Schwarz, Chem. Soc. Rev. 27 (1998) 91.
[13] F. Tureček, J. Mass Spectrom. 33 (1998) 779.
[14] D.V. Zagorevskii, J.L. Holmes, Mass Spectrom. Rev. 18 (1999) 87.
[15] R.A. Kelly, Atomic and ionic spectrum lines below 2000 Angstroms: hydrogen through krypton. Part I (H-Cr). American Chemical Society, New York, 1987, J. Phys. Chem. Ref. Data, 16 (Suppl. 1) 22, 161, 419.
[16] S. Beranova, C. Wesdemiotis, J. Am. Soc. Mass Spectrom. 5 (1994) 1093.
[17] S. Hayakawa, Int. J. Mass Spectrom. 212 (2001) 229.
[18] V.Q. Nguyen, F. Tureček, J. Mass Spectrom. 31 (1996) 843.
[19] S. Buchau, R.F. Porter, J. Phys. Chem. 95 (1991) 1139.
[20] S. Buchau, R.F. Porter, Chem. Phys. Lett. 170 (1990) 415.
[21] M. Sadílek, F. Tureček, Chem. Phys. Lett. 263 (1996) 203.
[22] M. Sadílek, F. Tureček, J. Phys. Chem. 100 (1996) 9610.
[23] V.Q. Nguyen, M. Sadílek, A.J. Frank, J.G. Ferrier, F. Tureček, J. Phys. Chem. A 101 (1997) 3789.
[24] J.K. Wolken, F. Tureček, J. Am. Chem. Soc. 121 (1999) 6010.
[25] J.K. Wolken, F. Tureček, J. Phys. Chem. A 103 (1999) 6268.
[26] P. Gerbaux, F. Tureček, J. Phys. Chem. A 106 (2002).
[27] P.J. Derrick, Mass Spectrom. Rev. 2 (1983) 285.
[28] W.L. Fitch, A.D. Sauter, Anal. Chem. 55 (1983) 832.
[29] F. Tureček, J.K. Wolken, M. Sadílek, Eur. Mass Spectrom. 4 (1998) 321.
[30] C. Lifshitz, Mass Spectrom. Rev. 1 (1982) 309.
[31] E. Uggerud, Adv. Mass Spectrom. 13 (1995) 53.
[32] F. Tureček, J. Phys. Chem. A 102 (1998) 4703.